Subwavelength broadband splitters and switches for femtosecond plasmonic signals

Andreas A. Reiserer[1], Jer-Shing Huang[2], Bert Hecht[2], and Tobias Brixner[1,*]

[1] *Institut fr Physikalische und Theoretische Chemie, Universitt Wrzburg, Am Hubland, 97074 Wrzburg, Germany*

[2] *Nano-Optics and Biophotonics Group, Physikalisches Institut, Department of Experimental Physics 5, Wilhelm-Conrad-Rntgen-Center for Complex Material Systems (RCCM), Universitt Wrzburg, Am Hubland, 97074 Wrzburg, Germany*

[*] *brixner@phys-chemie.uni-wuerzburg.de*

Abstract: Numerical simulations and an analytic approach based on transmission line theory are used to design splitters for nano-plasmonic signal processing that allow to arbitrarily adjust the ratio of transmission from an input into two different output arms. By adjusting the geometrical parameters of the structure, either a high bandwidth or a sharp transmission resonance is obtained. Switching between the two arms can be achieved by modulating the effective refractive index of the waveguide. Employing the instantaneous Kerr effect, switching rates in the THz regime are potentially feasible. The suggested devices are of interest for future applications in nanoplasmonic information processing.

OCIS codes: (250.5403) Plasmonics; (240.6680) Surface plasmons; (320.7085) Ultrafast information processing; (130.4815) Optical switching devices; (230.7380) Waveguides, channeled; (200.4560) Optical data processing; (350.4238) Nanophotonics and photonic crystals.

References and links

1. R. Zia, J. A. Schuller, A. Chandran, and M. L. Brongersma, "Plasmonics: the next chip-scale technology," Mater. Today **9** (7–8), 20–27 (2006).
2. W. L. Barnes, A. Dereux, and T. W. Ebbesen, "Surface plasmon subwavelength optics," Nature **424**, 824–830 (2003).
3. E. Moreno, S. G. Rodrigo, S. L. Bozhevolnyi, L. Martin-Moreno, and F. J. Garcia-Vidal, "Guiding and Focusing of Electromagnetic Fields with Wedge Plasmon Polaritons," Phys. Rev. Lett. **100**, 023901 (2008).
4. M. Quinten, A. Leitner, J. R. Krenn, and F. R. Aussenegg, "Electromagnetic energy transport via linear chains of silver nanoparticles," Opt. Lett. **23**, 1331–1333 (1998).
5. S. A. Maier, M. L. Brongersma, P. G. Kik, S. Meltzer, A. A. G. Requicha, and H. A. Atwater, "Plasmonics-A Route to Nanoscale Optical Devices," Adv. Mater. **13**, 1501–1505 (2001).
6. M. Sukharev and T. Seideman, "Coherent control of light propagation via nanoparticle arrays," J. Phys. B **40**, 283–298 (2007)
7. P. Tuchscherer, C. Rewitz, D. V. Voronine, F. J. García de Abajo, W. Pfeiffer, and T. Brixner, "Analytic coherent control of plasmon propagation in nanostructures," Opt. Express **17**, 14235–14259 (2009)
8. S. I. Bozhevolnyi and J. Jung, "Scaling for gap plasmon based waveguides," Opt. Express **16**, 2676–2684 (2008).
9. J.-S. Huang, T. Feichtner, P. Biagioni, and B. Hecht, "Impedance Matching and Emission Properties of Nanoantennas in an Optical Nanocircuit," Nano Lett. **9**, 1897–1902 (2009).
10. E. Verhagen, J. A. Dionne, L. Kuipers, H. A. Atwater, and A. Polman, "Near-Field Visualization of Strongly Confined Surface Plasmon Polaritons in Metal−Insulator−Metal Waveguides," Nano Lett. **8**, 2925–2929 (2008).
11. J. Grandidier, G. C. des Francs, S. Massenot, A. Bouhelier, L. Markey, J. Weeber, C. Finot, and A. Dereux, "Gain-Assisted Propagation in a Plasmonic Waveguide at Telecom Wavelength," Nano Lett. **9**, 2935–2939 (2009).

#126085 - $15.00 USD Received 26 Mar 2010; revised 10 May 2010; accepted 16 May 2010; published 19 May 2010

12. R. F. Oulton, V. J. Sorger, D. A. Genov, D. F. P. Pile, and X. Zhang, "A hybrid plasmonic waveguide for subwavelength confinement and long-range propagation," Nature Photon. **2**, 496–500 (2008).
13. D. J. Bergman and M. I. Stockman, "Surface Plasmon Amplification by Stimulated Emission of Radiation: Quantum Generation of Coherent Surface Plasmons in Nanosystems," Phys. Rev. Lett. **90**, 027402 (2003).
14. M. Ambati, S. H. Nam, E. Ulin-Avila, D. A. Genov, G. Bartal, and X. Zhang, "Observation of Stimulated Emission of Surface Plasmon Polaritons," Nano Lett. **8**, 3998–4001 (2008).
15. M. A. Noginov, G. Zhu, M. Mayy, B. A. Ritzo, N. Noginova, and V. A. Podolskiy, "Stimulated Emission of Surface Plasmon Polaritons," Phys. Rev. Lett. **101**, 226806 (2008).
16. P. Neutens, P. Van Dorpe, I. De Vlaminck, L. Lagae, and G. Borghs, "Electrical detection of confined gap plasmons in metal–insulator–metal waveguides," Nature Photon. **3**, 283–286 (2009).
17. G. Veronis and S. Fan, "Bends and splitters in metal–dielectric–metal subwavelength plasmonic waveguides," Appl. Phys. Lett. **87**, 131102 (2005).
18. A. V. Krasavin and A. V. Zayats, "Passive photonic elements based on dielectric-loaded surface plasmon polariton waveguides," Appl. Phys. Lett. **90**, 211101 (2007).
19. Z. Han and S. He, "Multimode interference effect in plasmonic subwavelength waveguides and an ultra-compact power splitter," Opt. Commun. **278**, 199–203 (2007).
20. S. Passinger, A. Seidel, C. Ohrt, C. Reinhardt, A. Stepanov, R. Kiyan, and B. Chichkov, "Novel efficient design of Y-splitter for surface plasmon polariton applications," Opt. Express **16**, 14369–14379 (2008).
21. Y. Matsuzaki, T. Okamoto, M. Haraguchi, M. Fukui and M. Nakagaki, "Characteristics of gap plasmon waveguide with stub structures," Opt. Express **16**, 16314–16325 (2008).
22. S. I. Bozhevolnyi, V. S. Volkov, E. Devaux, J. Laluet, and T. W. Ebbesen, "Channel plasmon subwavelength waveguide components including interferometers and ring resonators," Nature **440**, 508–511(2006).
23. Z. Kang and G. P. Wang, "Coupled metal gap waveguides as plasmonicwavelength sorters," Opt. Express **16**, 7680–7685 (2008).
24. J. A. Dionne, K. Diest, L. A. Sweatlock, and H. A. Atwater, "PlasMOStor: A Metal−Oxide−Si Field Effect Plasmonic Modulator," Nano Lett. **9**, 897–902 (2009).
25. C. Min and G. Veronis, "Absorption switches in metal–dielectric–metal plasmonic waveguides," Opt. Express **17**, 10757–10766 (2009).
26. W. Cai, J. S. White, and M. L. Brongersma, "Compact, High-Speed and Power-Efficient Electrooptic Plasmonic Modulators," Nano Lett. **9**, 4403–4411 (2009).
27. M. I. Stockman, S. V. Faleev, and D. J. Bergman, "Coherent Control of Femtosecond Energy Localization in Nanosystems," Phys. Rev. Lett. **88**, 067402 (2002).
28. M. Aeschlimann, M. Bauer, D. Bayer, T. Brixner, F. J. García de Abajo, W. Pfeiffer, M. Rohmer, C. Spindler, and F. Steeb, "Adaptive subwavelength control of nano-optical fields," Nature **446**, 301–304 (2007).
29. J. S. Huang, D. V. Voronine, P. Tuchscherer, T. Brixner, and B. Hecht, "Deterministic spatiotemporal control of optical fields in nanoantennas and plasmonic circuits," Phys. Rev. B **79**, 195441 (2009).
30. W. H. A. Schilders, P. G. Ciarlet, J. Lions, and E. J. W. T. Maten, *Numerical Methods in Electromagnetics* (Elsevier, 2005).
31. U. Inan and A. Inan, *Engineering electromagnetics* (Addison-Wesley, 1999).
32. Lumerical FDTD solutions, version 6; www.lumerical.com
33. E. D. Palik and G. Ghosh, *Handbook of optical constants of solids* (Academic Press, 1985).
34. K. F. MacDonald, Z. L. Samson, M. I. Stockman, and N. I. Zheludev, "Ultrafast active plasmonics," Nature Photon. **3**, 55–58 (2009).
35. R. Trebino, *Frequency-resolved optical gating: The measurement of ultrashort laser pulses* (Kluwer Academic Publishers, 2000).
36. G. Lenz, J. Zimmermann, T. Katsufuji, M. E. Lines, H. Y. Hwang, S. Spälter, R. E. Slusher, S.-W. Cheong, J. S. Sanghera, and I. D. Aggarwal, "Large Kerr effect in bulk Se-based chalcogenide glasses," Opt. Lett. **25**, 254–256 (2000).
37. J. Güdde, J. Hohlfeld, J. G. Müller, and E. Matthias, "Damage threshold dependence on electron-phonon coupling in Au and Ni films," Appl. Surf. Sci. **127–129**, 40–45 (1998).
38. S. Kim, J. Jin, Y.-J. Kim, I.-Y. Park, Y. Kim, and S.-W. Kim, "High-harmonic generation by resonant plasmon field enhancement," Nature **453**, 757–760 (2008).

1. Introduction

Coupled oscillations of the electromagnetic field and the density of the free electron gas at a metal-dielectric interface, called surface plasmon polaritons (SPPs), provide means to effectively confine optical excitations in nanoscale volumes. In combination with the ability to manufacture metal nanostructures using electron beam lithography or focused ion beam milling this allows for the investigation and manipulation of electromagnetic fields at a length scale that

#126085 - $15.00 USD Received 26 Mar 2010; revised 10 May 2010; accepted 16 May 2010; published 19 May 2010

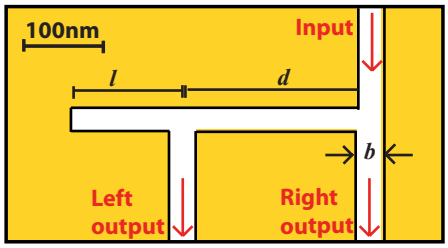

Fig. 1. Basic geometry of a 2D splitter structure. Waveguide modes are injected into the top arm (input). The electromagnetic fields are recorded in spectral and temporal domain by appropriate monitors in the left and right output arm. The frequency-dependent transmission and reflection are investigated for varying stub length l and distance d using a waveguide of gap width b.

is much smaller than the wavelength of light.

In particular, subwavelength plasmonic waveguides might lead to new information processing technology that combines the advantages of integrated electronics and photonics: high operating speed and small spatial extent [1]. Currently, various types of plasmonic waveguides are investigated in this context, including metal stripes [1, 2], wedges [3], nanoparticle arrays [4–7], and metal–insulator–metal (MIM) waveguides of different geometries [8–10]. All of these waveguides exhibit comparatively large damping of SPPs due to Ohmic losses in the metal. This, however, may be overcome by new concepts that enable low-loss plasmon propagation either by introducing a high-gain material into the waveguide [11] or by making use of the reduced damping in hybrid metal–semiconductor waveguides [12]. Moreover, nanoscale coherent plasmon sources [13–15] and detectors [16] as well as functional elements like splitters [17–21], multiplexers, frequency filters [22, 23] and switches [24–26] are being developed. Coherent control concepts also provide fascinating perspectives in the context of nanoplasmonic circuitry [6, 7, 27–29] since it provides full control over the temporal development and interference of all accessible Eigenmodes.

In the present work, signal splitters are proposed which owe their functionality to finite-length transmission line sections branching off a main line – so-called stubs [21]. We analyze these splitter structures by means of two-dimensional finite-difference time-domain (2D-FDTD) simulations [30] and compare the results to transmission line theory (TLT) [17, 31]. Since damping is included in our analytical model, the results of TLT provide a valuable guideline to find initial design parameters and trends which can then be further optimized by 2D-FDTD simulations.

In the basic design of a splitter structure that is proposed in this work, a stub of length l is attached at a distance d from a three-arm junction, as depicted in Fig. 1. As is well known from radiowave technology, this stub acts as an impedance connected in series to that of the left main line. The impedance of the stub can be tuned by changing its length [31] and width. It is therefore possible to arbitrarily adjust the transmission to either of the two output channels simply by choosing a suited geometry. A bandwidth of $25nm$ is achieved at a center wavelength of $800nm$, making the device capable of splitting femtosecond plasmon pulses. For a different choice of geometry, sharp transmission resonances are obtained which can be exploited to achieve both, frequency dependent splitting or active switching. The latter can be achieved by modulating the effective refractive index of the waveguide by employing any nonlinear effect.

In Sec. 2 we first describe the theoretical model and the simulation properties before we discuss the suggested broadband splitters in Sec. 3 and switches in Sec. 4.

#126085 - $15.00 USD Received 26 Mar 2010; revised 10 May 2010; accepted 16 May 2010; published 19 May 2010

2. Simulation properties and theoretical model

All simulations are done with a commercial software package [32]. We employ a subwavelength, single-mode, two-dimensional MIM (gold–vacuum–gold) waveguide as basic structure. This corresponds to a three-dimensional gap waveguide of large extent in the third dimension, as investigated in various studies [10, 16, 21, 24, 26]. The dielectric constant of gold is modeled by a fit to experimental data [33]. A mode source [32] injects the single guided mode. In order to obtain the frequency-dependent response function, we employ a broad Gaussian spectrum that corresponds to a $5fs$ (FWHM) laser pulse centered at a wavelength of $800nm$. Spectra are obtained by a Fourier transformation of the time-domain data and subsequent normalization to the source power [29]. A mesh spacing of $1nm$ is used in all simulations. Convergence checks lead to the conclusion that this is sufficient for accurate results. In order to absorb all energy at the edges of the simulation area, 100 perfectly matched layers [30, 32] (with the normalized imaginary electric and magnetic conductivity $\kappa = 200$ and the maximum normalized electric and magnetic conductivity $\sigma = 0.08$) are employed, leading to reflection coefficients of less than 10^{-4} over the complete investigated wavelength range ($700 - 900nm$).

With the goal to predict the geometry that is necessary to achieve certain transmission characteristics, transmission line theory (TLT) is employed. In the framework of TLT, which is routinely applied to microwave circuits, networks of transmission lines can be treated as circuits of interconnected impedances. As has been shown recently [9, 17, 21], TLT can also be used at optical frequencies to approximately determine e.g. reflection coefficients at subwavelength MIM waveguide junctions. The characteristic impedance Z_0 of the waveguide – defined as the ratio of current and voltage in a waveguide – is approximated by [17]

$$Z_0(b,\omega) \simeq \frac{Re\left[\gamma(b,\omega)\right]}{\omega\varepsilon_0} b. \tag{1}$$

Here, b is the width of the waveguide, ε_0 the free-space dielectric constant and ω the angular frequency of the guided plasmonic mode. $Re[]$ denotes taking the real part. γ is the complex propagation constant of the guided modes that determines the effective wavelength (imaginary part) and damping (real part) per unit length in a waveguide. Although Eq. (1) is an approximation to the true Z_0, it is found that the accuracy is sufficient to obtain reasonable agreement between TLT and FDTD-simulations. In particular Z_0 is real in this approximation, corresponding to a lossless line. This nevertheless yields reasonable results, since $Im[Z_0] \ll Re[Z_0]$. An alternative method of approximating the impedance of a certain waveguide is introduced in [9], which yields a complex impedance and is not restricted to 2D waveguides.

For real values of Z_0, the power reflection coefficient R at a load Z_{load}, connected to a waveguide of characteristic impedance Z_0, is given by [31]

$$R = \left| \frac{Z_{load} - Z_0}{Z_{load} + Z_0} \right|^2. \tag{2}$$

The input impedance of a waveguide of length l_{WG} that is terminated by Z_{load} is then [31]

$$Z_{in} = Z_0 \frac{Z_{load} + Z_0 \tanh\left(\gamma l_{WG}\right)}{Z_0 + Z_{load} \tanh\left(\gamma l_{WG}\right)}. \tag{3}$$

In this work, we will employ stub structures that consist of a waveguide of length l that is terminated by a short circuit [21], which means that $Z_{load} = 0$ in Eq. eq:InputImpedance. Thus, the input impedance $Z_{in,stub}$ of a stub consisting of a waveguide of characteristic impedance $Z_{0,stub}$ is given by

$$Z_{in,stub} = Z_{0,stub} \tanh\left(\gamma l\right). \tag{4}$$

#126085 - $15.00 USD Received 26 Mar 2010; revised 10 May 2010; accepted 16 May 2010; published 19 May 2010

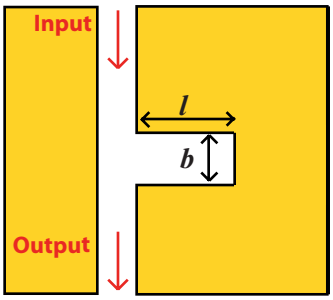

Fig. 2. Geometry for a series of simulations, where a stub of varying width b and length l is attached to a 30nm wide waveguide.

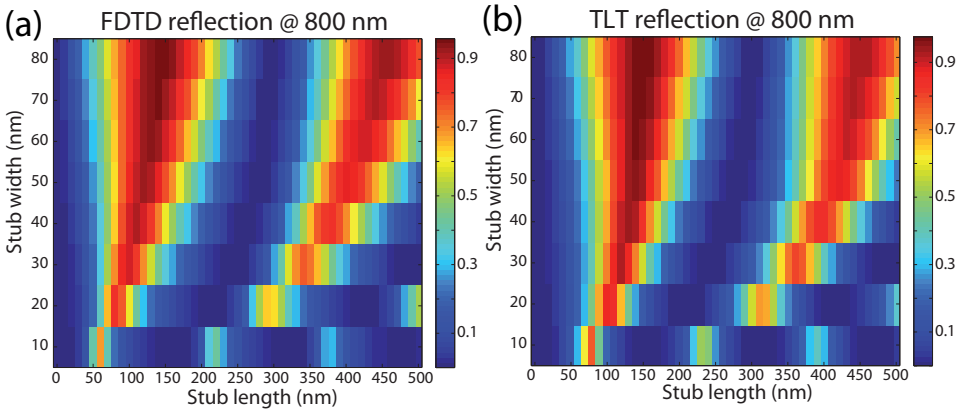

Fig. 3. FDTD (a) and TLT (b) reflection of a waveguide of 30nm width with an attached stub of varying width and length. The width of the reflection minima and maxima depends on the relative stub width.

Note that the input impedance is purely imaginary when Ohmic losses are neglected [21], since

$$Z_{0,stub}\tanh(\gamma l) = iZ_{0,stub}\tan(Im[\gamma]l), \tag{5}$$

where the characteristic impedance of the stub, $Z_{0,stub}$, is a real number. This means that no energy is absorbed inside the stub and all incident intensity will be transmitted or reflected. This approximation [Eq. (5)] is useful only for small stub lengths and large wavelengths. However, in real structures, the damping has to be included to provide accurate results. Therefore, the real and imaginary part of γ has been obtained for several waveguide widths b and wavelengths using a mode solver [32]. This in combination with Eq. (1) allows us to include the damping in the stub structures in the theoretical model and to compare FDTD simulation results with TLT for arbitrary geometrical parameters.

As a first step towards the proposed splitter structure, the influence of the width of an attached stub on the transmission and reflection has been studied in a set of simulations, where a single stub is attached to a waveguide of 30nm width, as depicted in Fig. 2. Subsequently, the stub width has been varied between 10 and 80nm and its length between 0 and 500nm – both in steps of 10nm.

In Fig. 3, the reflection is plotted as a function of stub width and length for the FDTD sim-

#126085 - $15.00 USD Received 26 Mar 2010; revised 10 May 2010; accepted 16 May 2010; published 19 May 2010

ulation [Fig. 3(a)] as well as for TLT [Fig. 3(b)]. We observe that the shape of the reflection maxima depends on the stub width. Thinner (thicker) stubs lead to sharper transmission minima (maxima). Thus, the width of the transmission resonance can be tuned by an appropriate choice of the stub width with respect to the extent of the waveguide.

The FDTD and TLT images show qualitative agreement, leading towards the conclusion that the chosen analytical approximation for Z_0 is reasonable and TLT can also be applied to approximate the transmission characteristics of stub structures of different width than the waveguide they are attached to. However, the FDTD reflection minima and the transmission maxima (not shown) are a little broader than expected from TLT. In spite of these deviations, we believe that TLT is useful for the design of nanoplasmonic functional elements. It provides an intuitive model that allows to understand the response of the investigated structures and to analyze the underlying mechanisms. Although accurate quantitative predictions are not possible, one can use TLT to calculate an approximate spectral response of a certain structure that can be used as a starting point for FDTD optimizations, which then give accurate results. We have employed TLT to identify the main geometrical parameters to implement the different functionalities of splitter structures that will be presented in the following.

3. Broadband splitters

In this section, we show how the reflection coefficient and the transmission ratio in the splitter device depicted in Fig. 1 can be manipulated by varying characteristic geometrical parameters of the structure. For simplicity, the stub and waveguide width are chosen identical in this section, so $Z_{0,stub} = Z_{0,waveguide} \equiv Z_0$.

In order to obtain the input impedance $Z_{in,splitter}$ of the whole structure, we substitute for Z_{load} in Eq. (3) the sum of the input impedance of the stub [calculated with Eq. (4)] and the impedance of the left waveguide (Z_0), and we consider the correct distance d. Thus we obtain

$$Z_{in,splitter} = \frac{1+\tanh(\gamma d)+\tanh(\gamma l)}{1+\tanh(\gamma d)\left[1+\tanh(\gamma l)\right]} Z_0. \tag{6}$$

We then calculate the reflection $R_{splitter}$ by inserting for Z_{load} in Eq. (2) the sum of the two input impedances at the first junction, i.e. the value from Eq. (6) for the left part and Z_0 for the right part. Thus we arrive at

$$R_{splitter} = \left| \frac{1+\tanh(\gamma d)+\tanh(\gamma l)}{3+\tanh(\gamma l)+\tanh(\gamma d)\left[3+2\tanh(\gamma l)\right]} \right|^2. \tag{7}$$

Note that this expression depends only on the waveguide parameter γ and the geometry. A waveguide intersection corresponds to a series connection of the output impedances, known from classical TLT [31]. Therefore, to obtain the transmission to one arm of the junction, one has to divide the real part of its impedance by the real part of the load, which in the present configuration corresponds to the sum of the impedances of both arms. For the right arm in Fig. 1, this yields

$$T_{rightarm} = \left(1-R_{splitter}\right) Re\left\{ \frac{1+\tanh(\gamma d)\left[1+\tanh(\gamma l)\right]}{\left[2+\tanh(\gamma l)\right]\left[1+\tanh(\gamma d)\right]} \right\}. \tag{8}$$

For the left arm comprising the stub, the transmission is calculated for both intersections consecutively. The damping upon propagation in between the intersections is included in the model by a multiplication with $e^{-Re[\gamma]d}$. For the left arm in Fig. 1, this leads to

$$T_{leftarm} = \left(1-R_{splitter}\right) Re\left\{ \frac{1+\tanh(\gamma d)+\tanh(\gamma l)}{\left[2+\tanh(\gamma l)\right]\left[1+\tanh(\gamma d)\right]} \right\} e^{-Re[\gamma]d} Re\left\{ \frac{1}{1+\tanh(\gamma l)} \right\}. \tag{9}$$

#126085 - $15.00 USD Received 26 Mar 2010; revised 10 May 2010; accepted 16 May 2010; published 19 May 2010

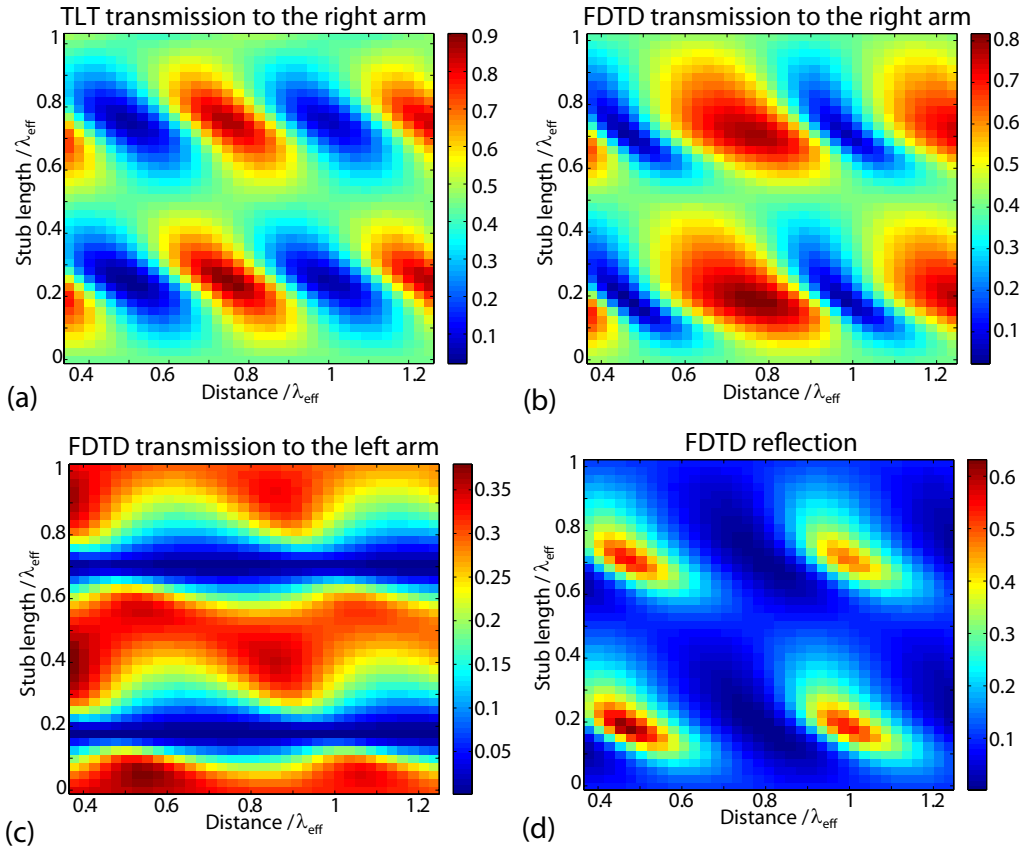

Fig. 4. Transmission to the right arm (a: TLT, b: FDTD), left arm (c), and reflection (d) of the splitter structure shown in Fig. 1. All data are shown as a function of the stub length and its distance from the intersection.

From the results calculated with Eq. (7), (8) and (9), one expects that the transmission to both arms strongly depends on the stub length and its distance from the junction. A corresponding plot of the transmission to the right arm is shown in Fig. 4(a). The axes are rescaled to the effective plasmonic wavelength $\lambda_{eff} = \frac{2\pi}{Im[\gamma]}$ of the guided mode that depends on the imaginary part of the propagation constant $Im[\gamma]$ and, thus, on the material and geometry of the waveguide. The analytical model is compared to a set of 2D FDTD simulations at a wavelength of 700nm, depicted in Fig. 4(b). Qualitative agreement can be seen regarding the position and amplitude of the minima and maxima. However, the FDTD transmission maxima are broader and shifted. In Figs. 4(c) and 4(d), the FDTD transmission to the left arm and the overall reflection are shown, respectively. Also here, qualitative agreement between simulation and theory is observed (not shown).

At its maximum, the transmission reaches $\sim 40\%$ to the left arm comprising the stub [red areas in Fig. 4(c)] and $\sim 80\%$ to the other arm [red areas in Fig. 4(b)]. The sum of the transmission to both arms is larger than 70% for most of the investigated geometries, making the splitter device quite effective given the large propagation loss in nanoplasmonic waveguides. The structure can be used to adjust the ratio of reflection and transmission to each arm by choosing an appropriate geometry for which the ratio of the input impedance of the left arm and the characteristic impedance of the right arm corresponds to the desired transmission ratio.

#126085 - $15.00 USD Received 26 Mar 2010; revised 10 May 2010; accepted 16 May 2010; published 19 May 2010

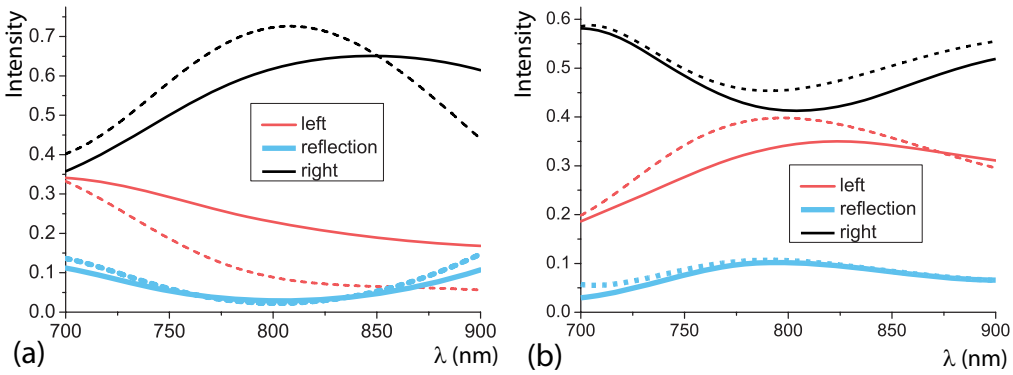

Fig. 5. TLT (dashed) and FDTD (solid) reflection (thick, light blue) and transmission to the left (red) and right (black) arm of a splitter structure consisting of 30*nm* wide waveguides. Two examples are depicted: (a) $l = 170nm$, $d = 320nm$, $\frac{T_{right}}{T_{left}} \simeq 2.5$. (b) $l = 240nm$, $d = 350nm$, $\frac{T_{right}}{T_{left}} \simeq 1.2$.

The proposed splitter provides the major advantage of plasmonics with respect to information processing: It can operate at a very high bandwidth. This can be seen in the two examples of Fig. 5, where a 170*nm* [Fig. 5(a)] or 240*nm* [Fig. 5(b)] long stub has been attached at a distance of $\sim \frac{3\lambda_{eff}}{4}$ from a junction, as depicted in Fig. 1. The two stub lengths show exemplary transmission ratios between right (black) and left (red) output of 2.5 [Fig. 5(a)] or 1.2 [Fig. 5(b)] at 800*nm*, while the reflection (thick, light blue) remains small. This illustrates the broad range of tunability in splitting ratios.

In both depicted structures, the analytically calculated (dashed) and the FDTD (solid line) reflection (thick, light blue) and transmission to the left (red) and right (black) arm remain quite constant over a range of more than 25*nm* around the center wavelength of $\sim 800nm$. This means that the device is capable of splitting near-infrared plasmonic signals in the femtosecond regime without major bandwidth-related pulse distortions. Note that a comparably high bandwidth is also achievable at any other splitting ratio. For this purpose it is important to choose both the stub length and the distance to the junction as small as possible for the intended ratio, so that the effective length $\frac{l}{\lambda_{eff}}$ and distance $\frac{d}{\lambda_{eff}}$ will vary as little as possible for different frequencies. Short distances are advantageous in any case because losses are minimized and maximal miniaturization is achieved. However, the use of long stubs also allows for applications that require a frequency-dependent split. This will be discussed in more detail below.

In addition to its high bandwidth, the proposed structure offers several advantages compared to other splitter geometries [17–21]. It is to our knowledge the smallest device that allows for an arbitrary-ratio split of ultrafast plasmonic signals on a nanoscale and with low back reflection. Moreover, its design is quite simple, and compatible with current nanofabrication techniques.

The working principle of the structure can be generalized to more complex designs. It is, e.g., possible to split a signal to two waveguides of different width and adjust the transmission ratio: The formulas for the input impedance of the splitter can easily be modified for waveguides of different impedances and the obtained values can be used to tune the stub length as mentioned above. If low back reflection is of high importance, even better results are achievable with a second stub that is attached to the other (right) arm. This allows to modify the input impedance of both arms in such a way that their sum equals the characteristic impedance of the input waveguide and, thus, $R = 0$ in Eq. eq:RefCoeff. However, this will increase the dimensions of the splitter structure and the losses. Since it might also lead to a reduced bandwidth and

#126085 - $15.00 USD Received 26 Mar 2010; revised 10 May 2010; accepted 16 May 2010; published 19 May 2010

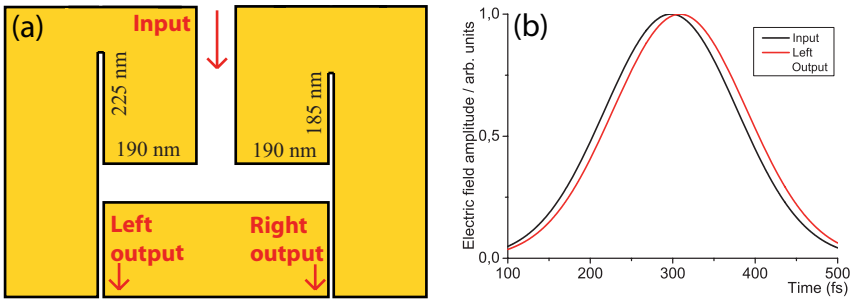

Fig. 6. (a) Geometry of the proposed switch. Plasmons are injected by a mode source in the upper arm (input). The electromagnetic fields are recorded in the input, left and right output arm. (b) Electic field amplitude of a $200\,fs$ Gaussian-envelope plasmonic signal before (black) and after (red) the switch. No significant phase-related pulse broadening can be observed.

complicate the fabrication of the structure, the easier design comprising one arm is probably better suited for most applications.

4. Wavelength dependent splitters and switches

In the following, the application of the proposed splitter structure as a switch for femtosecond plasmonic signals on a nanoscale is investigated. The working principle is to shift the spectral transmission maximum in a structure with a steep wavelength dependent transmission curve by varying the effective stub length $\frac{l}{\lambda_{eff}} = n_{eff}\frac{l}{\lambda_0}$ on a fast timescale. This in turn can be achieved by a modification of the effective index n_{eff} of the terminated waveguide, e.g. by a variation of the index of the insulating core using the Kerr effect or an active medium in the gap [26]. As well, a DC voltage or a manipulation of the dielectric constant of the metal via a coherent nonlinearity [34] might be employed. We note that the nonresonant optical Kerr effect offers a quasi-instantaneous response which is a reason for its usefulness in femtosecond laser pulse characterization [35]. Hence also in our case the Kerr effect in principle allows ultrafast switching.

Since the change in n_{eff} is usually limited to a few percent, steep transmission resonances are required to achieve switching; these can be achieved in splitters if a thin stub is attached to a thicker waveguide. In the following, the working principle of the proposed device is illustrated by means of FDTD simulations. For this purpose, a splitter (stub and output waveguide width: $10nm$; input waveguide width: $80nm$) is investigated where a dielectric material of refractive index $n = 1$ forms the insulator of a two-dimensional MIM waveguide. A stub is attached to each arm of the structure as depicted in Fig. 6(a). In Fig. 6(b), a $200\,fs$ Gaussian-envelope plasmonic signal is shown before (black) and after (red) passing through this structure. Since both the spectral transmission and the spectral phase response of the structure are rather flat, almost no pulse broadening is observed.

As mentioned, the output power to the arms of the splitter is dependent on the ratio of their impedances. Therefore, the geometry has been chosen in such a way that for $n = 1$, $\lambda = 810nm$, the impedance of the left arm takes a very high value, while it is small for the right arm. This leads to a high transmission to the left arm. However, when the refractive index is changed by 5%, the effective stub length changes in such a way that the input impedance of the right arm gets much smaller, while that of the left arm increases. Therefore, the transmission is switched to the right arm.

#126085 - $15.00 USD Received 26 Mar 2010; revised 10 May 2010; accepted 16 May 2010; published 19 May 2010

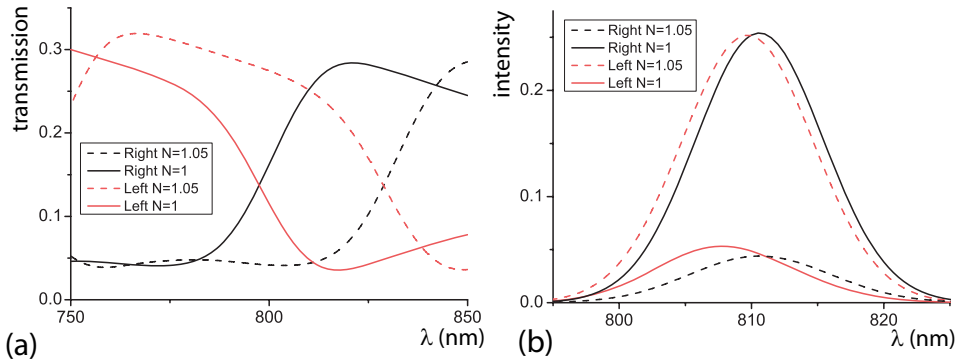

Fig. 7. (a) Transmission to the left (red) and right (black) arm of a splitter structure upon variation of the refractive index from $n = 1$ (solid) to $n = 1.05$ (dashed). (b) Spectral intensity at the left (red) and right (black) output when a Gaussian plasmon pulse of 5*nm* FWHM impinges on the splitter. Most of the intensity is transmitted to the right arm in the case $n = 1$ (black solid), while it is transmitted to the left arm for $n = 1.05$ (red dashed).

This is illustrated by two simulations. In Fig. 7(a), the transmission curve to the left (red) and right (black) arm of a splitter structure is shifted when the refractive index of the core is changed from $n = 1$ (solid line) to $n = 1.05$ (dashed). The transmitted intensity of a $200\,fs$ (FWHM) plasmon pulse centered around $\lambda = 810nm$ is depicted in Fig. 7(b); it has been calculated by a multiplication of the input spectrum with the spectral transmission [shown in Fig. 7(a)]. It can be clearly seen that the transmission ratio between right and left output is switched from 6:1 ($n = 1$) to 1:6 ($n = 1.05$).

As already mentioned, the working principle of the proposed switch is not restricted to a certain kind of nonlinearity. In the structure discussed above, an increase in the refractive index of 5% is sufficient for switching. However, this value can be further reduced when longer stubs are used – at the price of a reduced bandwidth, larger spatial extent and higher losses. The design of real functional elements therefore has to be adjusted to the magnitude of the nonlinearity. Combination of the nanostructure with suitable materials of high Kerr nonlinearity can make the 5% change feasible. We can calculate the achievable index change Δn via $\Delta n(t) = n_2 I(t)$, where n_2 is the Kerr coefficient and $I(t)$ the optical intensity. As an example for large-Kerr-effect materials, n_2 values for Se-based chalcogenide glasses have been reported up to 500 times larger than for regular SiO_2 glass, reaching $1.7 \times 10^{-13} cm^2$/W [36]. Requesting $\Delta n = 0.05$ with such a material, a peak intensity of 3×10^{11} W/cm^2 would be required. At a switching-pulse duration of 200 fs (corresponding to the bandwidth of the switching device) and an effective area of $(400nm)^2$ (roughly corresponding to the size of the device), we can thus estimate the required pulse energy to be 100 pJ. We expect this should be feasible without introducing damage [37, 38]. This is true especially since the local field enhancement of the nanostructure leads to a further reduction of the required switching-pulse energy. Intensity enhancements of two orders of magnitude over length scales of 1000 nm have been observed [9].

Since the spectral bandwidth of the switchable plasmon signal corresponds to a pulse duration of $200\,fs$ and the Kerr effect is quasi-instantaneous [35], switching might be possible on a timescale of $200\,fs$. MacDonald et al. have also observed reaction times below $200\,fs$ [34]. The dispersion properties of the material are of little concern for possible pulse-shape modifications because the propagation length is so short, see also Fig. 6(b). Thus the maximum achievable rate is estimated to be in the range of a few THz – three orders of magnitude faster than current electronic devices. Further experimental and theoretical investigations are required to deduce

#126085 - $15.00 USD Received 26 Mar 2010; revised 10 May 2010; accepted 16 May 2010; published 19 May 2010

the ultimate limit on the maximum achievable speed of operation.

5. Summary

In conclusion, it has been shown that stubs can be applied to design nano-scale power-efficient arbitrary ratio splitters that provide the major advantages of plasmonic devices – high operating speed and small spatial extent. The spectral response can be tuned by changing the width and length of the stubs. By changing the refractive index in a structure with sharp spectral response, switching can be achieved with a comparably high bandwidth. In contrast to previously proposed plasmon switches [24–26], the structures that are investigated in this work can be used to switch the incident energy between either of two output channels. The achievable switching speed is limited by the timescale of the refractive index change and the switching bandwidth. For the structure analyzed here and the instantaneous Kerr effect, switching rates in the THz regime should be possible in principle, three orders of magnitude faster than what is achievable with current electronic devices. Future experimental studies on plasmon propagation in subwavelength waveguides are likely to show the feasibility of the proposed concepts.

Acknowledgments

We acknowledge financial support from the DFG (SPP 1391 “Ultrafast Nanooptics”). P. Tuchscherer, C. Rewitz and P. Biagioni are acknowledged for helpful discussions.

#126085 - $15.00 USD Received 26 Mar 2010; revised 10 May 2010; accepted 16 May 2010; published 19 May 2010